Citation for published version:
Liu, Z, Koh, KL, Mezentsev, A, Enno, SE, Sugier, J & Fullekrug, M 2018, 'Lightning Sferics: Analysis of the Instantaneous Phase and Frequency Inferred From Complex Waveforms', Radio Science, vol. 53, no. 4, pp. 448-457. https://doi.org/10.1002/2017RS006451

DOI:
10.1002/2017RS006451

Publication date:
2018

Document Version
Peer reviewed version

Lightning Sferics: Analysis of the Instantaneous Phase and Frequency Inferred from Complex Waveforms

Zhongjian Liu[1], Kuang Liang Koh[1], Andrew Mezentsev[2], Sven-Erik Enno[3], Jacqueline Sugier[3], and Martin Fullekrug[1]

[1] Centre for Space, Atmospheric and Oceanic Science, University of Bath, Bath, United Kingdom.

[2] Birkeland Centre for Space Science, University of Bergen, Bergen, Norway.

[3]Remote Sensing (Lightning, Clouds, Aerosols), and Aircraft Based Observation R&D, Met Office, Exeter, United Kingdom.

Corresponding author: Zhongjian Liu (z.liu@bath.ac.uk)

Key Points:

- A complex waveform bank and a spectral waveform bank has been produced from lightning sferics.
- Long-range lightning location systems achieve sub-sampling time accuracy using the instantaneous phase of complex lightning sferic waveform.
- The instantaneous frequencies at maximum amplitudes are distance dependent.

Abstract

Analysis of VLF lightning waveforms, or radio sferics, can contribute to research into lower ionosphere perturbations and the corresponding atmospheric chemistry. Lightning waveforms can also be characterized on the basis of their propagation distance from receivers in order to study radio wave propagation. A bank of average waveforms, i.e. the waveform bank, <1,000 km with a spatial resolution of 10 km has been produced, based on the lightning waveforms recorded in Europe on 8th August 2014. These average lightning waveforms at different distances exhibit a sequence of consecutive maxima resulting from ionospheric reflections, named sky waves. The spectral waveform bank shows a sequence of consecutive modal maxima at different frequencies depending on distance. The Hilbert transform is applied to produce complex lightning waveforms, which provide additional information to the original real waveforms alone, i.e., the instantaneous phase and frequency. The time differences calculated from the instantaneous phases of complex lightning waveforms gives the minimum arrival time difference error when compared to other analyzed signal processing methods. The derivative of the instantaneous phase, i.e. the instantaneous frequency, represents the amplitude-weighted average of frequency components at maximum amplitude according to theory and numerical simulation. In real experiments, the instantaneous frequency can be understood as the median value of the real frequency distribution calculated at maximum amplitude. It is found that the instantaneous frequencies at maximum amplitudes are distance dependent. This finding might enable the development of a novel method to determine lightning distances in the future.

1 Introduction

Lightning is the strongest natural electromagnetic radiation source in the earth's atmosphere and it emits electromagnetic waves in the frequency range from ~1 Hz to >300 MHz [e.g., *Rakov and Uman, 2003; Rison et al., 2016*]. Ground-based lightning location systems are essentially based on the received electromagnetic waves and subsequent signal processing [*e.g., Dowden et al., 2002; Holler et al., 2009; Bitzer et al., 2013; Rakov, 2013; Stock et al., 2014; Lyu et al., 2014; Nag et al., 2015; Wang et al., 2016; Sun et al., 2016*]. For example, the azimuth of an incident radio wave from a lightning discharge is determined by calculating the voltage ratio received by two magnetic loop antennas, named magnetic direction finding (MDF) [*e.g., Horner, 1954, 1957; Krider et al., 1976; Fullekrug et al., 2000*]. In the most commonly used lightning location method, arrival time differences (ATD) are extracted by different signal processing techniques from the lightning waveforms recorded at different radio receiver stations [e.g. *Lee, 1986, 1990; Cummins et al., 1998, 2009*]. The different signal processing techniques result in slightly different arrival times with different corresponding lightning locations [*Liu et al., 2016*]. Using a different time extraction point, e.g. the waveform peak or rising edge, and different data pre-processing, e.g. wide or narrow bandwidth or complex envelope, can all introduce slightly varying time differences. As a result, a better understanding of the sferic, i.e. the received broadband lightning waveform, is a prerequisite for improving lightning location accuracy.

Much research into ionosphere perturbations and atmospheric chemistry utilize broadband VLF waveforms, in particular lightning waveforms [e.g. *Cheng et al., 2007; Shao et al., 2013*]. The sferic is a broadband electromagnetic impulse generated by a lightning discharge, which propagates through the earth-ionosphere waveguide. The perturbations in the D-region caused by the variation of electron densities will change the received sferic in the time and frequency domain. A collection of average lightning waveforms at different distances, named waveform bank, was introduced by Said et al. [*2010*]. This method offers an opportunity to characterize sferics and to estimate arrival times. This idea has been adopted and it is extended in this work to produce a new type of waveform bank for further analysis.

The time-dependent sferic signal is treated as an analytic signal, or complex trace, to process the received signal to determine the instantaneous phase and frequency at each sample in the time series [e.g. *Taner et al., 1979*]. It is more common to use the Fast Fourier Transform (FFT), or a Short-Time Fourier Transform (STFT), to calculate phases from the spectral coefficients at the harmonic frequencies $f_k = k/T$, where k is the harmonic number and T is the length of the time interval used for the FFT or STFT. As a result, the phases inferred from the FFT or STFT represent average values over the time interval $T = N\Delta t$, where N is the number of samples in that time interval and Δt is the sampling time interval. Given that the phase of a lightning sferic is constantly changing (Fullekrug et al., 2016, Fig 2, right), an averaged phase can include unwanted information that is introduced, for example, by the phase change during the time interval T, or by unwanted interference during that time interval. It is therefore interesting to investigate how useful the instantaneous phase of a lightning sferic is which is determined for each individual sample and which should have the smallest possible bias introduced by unwanted information. Therefore, this method will be applied here to a new lightning waveform bank (<1000 km) produced from data collected by a long-range lightning location system described below. The timing accuracy of the instantaneous phase is compared with other methods by using the speed of light as a reference. The derivative of the instantaneous phase is the instantaneous frequency, which is used to study the relationship with the real frequency of the sferic determined by its spectrum. The observed instantaneous frequency changes in the complex waveform bank are discussed and related to the radio wave propagation with distance.

2 The Complex Waveform Bank

2.1 The waveform bank

Previous research associated with sferic waveform characteristics, including polarity estimation, cycle errors and peak current, has shown that received lightning waveforms that originate from a certain storm cluster exhibit similar features [*Said et al., 2010, Figure 1*]. Thus, a small deviation of lightning waveform shape indicates a propagation over similar distances. A representative waveform is calculated by averaging each of the lightning waveforms in one distance bin to reduce the noise in each average waveform and to acquire a more pure lightning waveform that includes subtle propagation effects. Comparing the representative waveforms at different distances is an effective method to study the propagation effects on lightning sferics.

Lightning locations are reported by the French lightning detection network Meteorage, which covers south-western Europe and the western Mediterranean Sea. This network distinguishes cloud to ground lightning and intra-cloud lightning based on a linear discriminant analysis (LDA) of different waveform parameters, and the classification accuracy reaches 95% for negative cloud to ground lightning in France [*Kohlmann et al., 2017*]. The electromagnetic waveforms of the lightning discharges were recorded from ~21:00 UT 8th to ~03:00 UT on 9th August 2014 with four wideband digital low-frequency radio receivers located in Bath

(BTH), Orleans (ORL), Lannemezan (LMZ), and Rustrel (RST) [*Liu et al., 2016*]. The radio receiver records the electric field from a capacitive probe with a sampling frequency of 1 MHz, an effective bandwidth from ~4 Hz to ~400 kHz and a timing accuracy of ~12 ns provided by a GPS disciplined frequency standard [*e.g. Fullekrug, 2010,; Fullekrug et al. 2006, 2014, 2015; Mezentsev et al., 2013; Soula et al., 2014*].

During the 7 hour long recording, more than 150,000 cloud to ground (CG) lightning stroke waveforms from a mesoscale convective system over central France were recorded by the four sensors with peak currents ranging from -4 kA to -40 kA, which were located 0-1000 km away from each radio receiver [*Liu et al., 2016*]. The lightning waveforms ranging from -1 ms to +4 ms around the occurrence of the lightning discharges were extracted from the digital recordings based on the lightning locations and occurrence times reported by Meteorage. The time t=0 of the lightning waveforms is referenced to the propagation time at the speed of light calculated from the great circle distance between the source and the receiver. This referencing procedure enables the calculation of one average waveform for each distance bin with a width of 10 km. Each distance bin consists of at least one hundred lightning waveforms. The resulting 100 average waveforms form the lightning waveform bank form the basis for the subsequent data analysis (Figure 1, left). The difference between an average lightning source current and the interfering signals from the local noise environment, man-made noise and radio transmissions are thereby minimized. The ionospheric conditions for the propagation of these lightning waveforms are similar, because all of the lightning sferic waveforms propagated during nighttime from the source to the receiver.

The waveform bank exhibits an initial pulse from the ground wave and a sequence of subsequent maxima from the ionospheric reflections or multi-hop sky waves. The first arrival sky wave can be observed after ~100 km propagation and additional sky wave hops can be observed for longer distance propagation. The energy of the lightning signals propagated along the ground path attenuate with distance due to ground conductivity, while the energy of lightning signals from the ionospheric reflections are attenuated by longer propagation distances and the ionospheric D-layer conductivity. The waveform bank shows distance-dependent arrival times of the ground wave and ionospheric reflections, which can be explained by ray theory [e.g. *Schonland et al., 1940; Carvalho et al., 2017; Qin et al., 2017*]. The waveform bank shows the ground wave arrival at 0 ms and the sky wave arrivals at increasing time delays for shorter distances, which is in agreement with theoretical calculations that use a flat-earth model or a spherical earth model [*Schonland et al., 1940*].

A spectral waveform bank can be calculated by averaging the complex spectra of all waveforms at the same distance bin or from the spectra of the average lightning waveforms at each distance bin. Both averaging procedures produce exactly the same result (Figure 1, right). The spectral waveform bank exhibits a sequence of consecutive maxima in the frequency range up to 100 kHz. These consecutive relative maxima result from the constructive superposition of numerous wave propagation modes, named modal maxima in the following text. The modal maxima are separated from each other by distinct spectral minima that are characteristic for the distance between the lightning discharges and the radio receivers. These features of the spectral waveform bank result mainly from the lightning sferics and propagation effects because averaging the waveforms eliminates most of the interfering noise such that the best possible average lightning sferic waveform is obatined. The spectral waveform bank is useful for understanding the propagation effects with distance and it can be used for theoretical modeling of radio wave propagation.

2.2 Complex Waveforms

The time dependent radio signal can be treated as an analytic signal or complex trace. This allows the extraction of the envelope and instantaneous phase for each sample [*e.g. Taner et al., 1979; Liu et al., 2016*]. The complex trace can be obtained from the real valued recordings using the Hilbert transform. In practice, the complex waveform can be calculated from the real signal by doubling the positive frequency and by eliminating the negative frequency. This complex waveform is subsequently down converted by multiplying with a frequency shift operator $\boldsymbol{e^{-j\Delta\omega t}}$ that centers the spectrum at zero frequency. The shift frequency Δω is normally set as the harmonic frequency which contains most of the energy of the target signal. For example, the shift frequency of a radio transmission is normally the center frequency of its modulation. The shift frequency of lightning can be set as 10 kHz as the return stroke deposits most of its energy around this frequency [*Fullekrug et al., 2013*]. The final complex waveform can be determined after applying a low-pass filter to the down converted signal in order to increase the signal to noise ratio

$$\boldsymbol{F(t)} = \left(\boldsymbol{f(t)} + \boldsymbol{jH}\big(\boldsymbol{f(t)}\big)\right) e^{-j\Delta\omega t} = \boldsymbol{A(t)e^{j\varphi(t)}} \qquad (1)$$

where, $\boldsymbol{A(t)}$ is the time dependent amplitude envelope and $\boldsymbol{\varphi(t)}$ is the time dependent instantaneous phase.

In this way, the complex waveform bank can be calculated from a real waveform bank by use of the Hilbert transform. The complex waveform from 2-18 kHz of an average lightning signal at 300 km is shown in figure 2. This three-dimensional trace of a lightning waveform illustrates the amplitude envelope and instantaneous phase variation over time. In the beginning, the phase of the complex trace is chaotic and the amplitude is low when there is no lightning signal. The arrival of ground wave and sky waves lead to large signals, which are well above the noise. These large signals result from a strong lightning discharge, so that the amplitude is increased and the phase is moved towards a specific value. In this example, the complex waveform rotates anticlockwise, which means that the instantaneous phase is decreasing during the pulse arrival. The signal returns to chaotic behavior after the lightning event.

3 Instantaneous Phase

Different information can be extracted from the complex waveform than from the real-valued signal, including the envelope of the complex trace and the instantaneous phase. The time differences calculated from the instantaneous phase between two lightning waveform peaks can be extracted by use of the transfer function calculated from the ratio between the two complex values at the peak of the waveform. Normally, the time difference between two lightning waveforms is constrained by the sampling frequency. In order to achieve the sub-sample time difference $\delta t = \delta\varphi/\omega$, the two waveforms are time shifted first in order to superpose the amplitude peaks. The instantaneous phase difference $\delta\varphi$ can then be extracted from the transfer function at the peak samples of the two waveforms $\delta\varphi = \varphi_{\max1} - \varphi_{\max2}$. This time difference inferred from the instantaneous phase achieves sub-sampling accuracy after taking into account cycle ambiguities, if any.

The propagation time delay relative to the speed of light using different signal processing methods can be compared by using the lightning waveform bank. The average lightning waveforms from 310 km to 600 km are compared with the average waveform at 300 km by using four different time extraction methods (Figure 3). The time offset δt is the measured time difference Δt minus the nominal time difference calculated for a propagation velocity at speed of light $\Delta t = \Delta d/c$, where Δd is the distance difference with respect to the lightning sferic waveform at 300 km distance, i.e., Δd = d-300 km with d ranging from 310 km to 600 km. All these methods determine the time offset that is measured with reference to the propagation time between the source and the receiver at the speed of light. The first three methods extract the occurrence times by waveform cross correlation, from the peak of the filtered data (5-15 kHz), and from the peak envelope of the complex trace. The average values of the absolute time offsets over all distance differences from 10-300 km with respect to the speed of light by using these three methods are ~2.33 μs, ~2.63 μs and ~4.23 μs, respectively, with corresponding ranges of [-3, 6] μs, [-4, 5] μs and [-8, 11] μs. The average value of the absolute time offset by measuring time differences with the instantaneous phase is only ~2.08 μs with a corresponding range [-2.78, 5.62] μs (Figure 3). In the case of a lightning location system using a propagation velocity at the speed of light, the time accuracy is therefore slightly improved by calculating the instantaneous phase from the complex waveform. The time offsets at different distances are neither constant nor distance dependent, which is suggested to be investigated in future analyses. One possible reason is the inappropriate presupposed wave propagation velocity in comparison, i.e. the speed of light, because it is found that the lightning electromagnetic wave may propagate at a varying phase propagation velocity [Liu et al., 2016].

4 Instantaneous Frequency

The different rotation direction of complex waveforms may indicate a different elevation angle of the incident lightning sferic [*Fullekrug et al., 2016, Figure 2, right*]. The rotation direction is the polarity of the derivative of the instantaneous phase in a complex waveform. This time dependent derivative $\boldsymbol{f_i = d\varphi/dt}$, is called the instantaneous frequency [*Taner et al., 1979*]. The instantaneous frequency indicates the phase change for each sample with reference to the center frequency of the signal. The rotation direction is anticlockwise when the instantaneous frequency is smaller than the center frequency and it is clockwise when the instantaneous frequency is larger than the center frequency. The benefit of using instantaneous frequency for range estimation is the high time resolution and also the frequency resolution. For example, the frequency resolution of the result from the STFT of a 1ms long time interval is only 1 kHz, without zero padding, while the instantaneous phase has a temporal resolution with the sampling time interval Δt = 1 **μ**s. The calculated result has no constraints on the frequency resolution within the passband of the low-pass filter applied to the down converted signal. A convenient way of computing the instantaneous frequency f_i from the complex trace C is to compute the derivative of the arctangent function

$$\boldsymbol{f_i = \frac{1}{2\pi}\frac{d}{dt}arctan\left(\frac{Im(C)}{Re(C)}\right),} \qquad (2)$$

which results in

$$\boldsymbol{f_i = \frac{Re(C)\dfrac{d(Im(C))}{dt} - Im(C)\dfrac{d(Re(C))}{dt}}{2\pi(Re(C)^2 + Im(C)^2)}} \,. \qquad (3)$$

A signal that consists of two frequency components, $\boldsymbol{f_1}$ and $\boldsymbol{f_2}$, is analysed in order to explore the relationship between the instantaneous frequency and the two frequency components. Assuming $\boldsymbol{C_1}$ and $\boldsymbol{C_2}$ are two single sinusoid complex signals, the instantaneous frequency of the superposed signal is

$$\boldsymbol{f_i = \frac{1}{2\pi}\frac{d}{dt}arctan\left(\frac{Im(C_1) + Im(C_2)}{Re(C_1) + Re(C_2)}\right)}, \qquad (4)$$

which results in

$$\boldsymbol{f_i = \frac{1}{2\pi}\frac{d}{dt}arctan\left(\frac{A_1 \sin\alpha + A_2 \sin\beta}{A_1 \cos\alpha + A_2 \cos\beta}\right)}, \qquad (5)$$

where $\boldsymbol{A_1}$ and $\boldsymbol{A_2}$ are the amplitudes of the two sinusoid signals and $\boldsymbol{\alpha}$ and $\boldsymbol{\beta}$ are the phases of the sinusoids $\boldsymbol{C_1}$ and $\boldsymbol{C_2}$. The derivatives of $\boldsymbol{\alpha}$ and $\boldsymbol{\beta}$ are $\boldsymbol{f_1}$ and $\boldsymbol{f_2}$. The explicit calculation of the derivative in equation 5 yields

$$\boldsymbol{f_i = \frac{(A_1 \cos\alpha + A_2 \cos\beta)(A_1 f_1 \cos\alpha + A_2 f_2 \cos\beta) + (A_1 f_1 \sin\alpha + A_2 f_2 \sin\beta)(A_1 \sin\alpha + A_2 \sin\beta)}{(A_1 \cos\alpha + A_2 \cos\beta)^2 + (A_1 \sin\alpha + A_2 \sin\beta)^2}}. \qquad (6)$$

In order to simplify this result, we assume that $\boldsymbol{\alpha} = \boldsymbol{\beta}$ when the amplitude of the superposed signal is maximal. In this case, it follows that

$$\boldsymbol{f_i = \frac{A_1 f_1 + A_2 f_2}{A_1 + A_2}}. \qquad (7)$$

Similarly, we assume that $\boldsymbol{\alpha = \pi + \beta}$ when the amplitude of the superposed signal is minimal. In this case, it follows that

$$\boldsymbol{f_i = \frac{A_1 f_1 - A_2 f_2}{A_1 - A_2}}. \qquad (8)$$

In the case where the instantaneous frequency of a signal consists of *N* frequency components

$$\boldsymbol{f_i = \frac{1}{2\pi}\frac{d}{dt}arctan\left(\frac{\sum_j^N A_j\, sin\,\alpha_j}{\sum_j^N A_j\, cos\,\alpha_j}\right)}, \qquad (9)$$

which results in

$$\boldsymbol{f_i = \frac{\left(\sum_j^N A_j f_j \cos\alpha_j\right)\left(\sum_j^N A_j \cos\alpha_j\right) + \left(\sum_j^N A_j \sin\alpha_j\right)\left(\sum_j^N A_j f_j \sin\alpha_j\right)}{2\pi\left(\left(\sum_j^N A_j \cos\alpha_j\right)^2 + \left(\sum_j^N A_j \sin\alpha_j\right)^2\right)}}, \qquad (10)$$

Where A_j are the amplitudes of the sinusoid signals and α_j are the phases of these sinusoids. The derivatives of α_j are the instantaneous frequencies f_j of the sinusoids. If the phases of all sinusoids are the same, i.e., $\alpha_j = \alpha \forall j$, then

$$\boldsymbol{f_i} = \frac{\sum_j^N \boldsymbol{A_j f_j}}{\sum_j^N \boldsymbol{A_j}}. \qquad (\mathbf{11})$$

These results show that the instantaneous frequency is equal to the amplitude-weighted frequency in the frequency domain when the amplitude of the complex signal is maximal. The instantaneous frequency may be singular when the denominator with the sum of amplitudes is zero.

The instantaneous frequency of two frequency components is confirmed by simulating a superposed signal $y = sin(2\pi * 100t) + 2sin(2\pi * 120t)$ (Figure 4). The signal is down converted by 110 Hz to compute the complex waveform. The instantaneous frequency is calculated directly from the derivative of the arctangent function (equation 3). The instantaneous frequency of a single sinusoid signal is a real constant frequency. The instantaneous frequency of the superposed signal varies depending on the amplitude of the complex waveform. The instantaneous frequency is equal to the amplitude-weighted average value calculated by equation 7 when the amplitude is maximal. The instantaneous frequency is not within the range of the two frequency components and equal to the result calculated by equation 8 when the amplitude is minimal. This simulation result confirms that the instantaneous frequency represents the amplitude-weighted average of the true frequencies in each sample when the amplitude is maximal. The instantaneous frequency provides no meaningful information about either of the two frequency components when the amplitude is minimal. Therefore, for a real wideband signal, such as lightning, the instantaneous frequency is only a reliable indicator of the true frequency spectrum when the amplitude is maximal.

5 Instantaneous Frequencies of Lightning Waveforms

The instantaneous frequency of the average lightning waveform at a distance of 300 km is calculated for different frequency bandwidths (Figure 5). At the beginning, the instantaneous frequency is chaotic due to the noise and large sensitivity of the instantaneous phase, and it is only relatively stable during the lightning pulses' arrival, which is confirmed by the simulation result in the previous section. In order to emphasize the results during maximum amplitude, the amplitude weighted average instantaneous frequency has been calculated by averaging n=20 samples of the dot product between the amplitudes and their instantaneous frequencies divided by the sum of all amplitudes. This amplitude weighted average of the instantaneous frequency with empirically selected n essentially is a moving average to avoid the frequency variation due to the sudden phase jump. While this moving average has tiny effect during lightning pulses, because the instantaneous frequency is stable at that period. This amplitude weighted average instantaneous frequency is likely to be of benefit for a detailed monitoring of the frequency distribution during the lightning period.

The instantaneous frequency of the average lightning waveform propagated over 300 km calculated from 2-18 kHz (Figure 2) shows that the instantaneous frequency is smaller than the center frequency of 10 kHz when the amplitude is maximum (Figure 5, upper left). This explains why the rotation direction of the complex waveform during lightning period is anticlockwise. The result means that the median value of the amplitude-weighted instantaneous frequency from 2-18 kHz during the lightning period is below 10 kHz according to the theoretical analysis explained in the previous section. However, there are several modal maxima in the spectra within this frequency range (Figure 1, right). Each peak in the spectrum may vary differently during the lightning period. As a result, it is better to concentrate on one modal maximum in the spectrum, so that the small variation of each peak during the lightning period can be observed individually. The instantaneous frequency calculated from a narrow-band frequency range around one peak in the spectrum is much less variable (Figure 5, lower left). The instantaneous frequency around the lightning pulse is almost constant, indicating that the frequency distribution during the lightning period is stable. It is noted that the stability of instantaneous frequency is more important than the value of instantaneous frequency, because the averaging value of the frequency distribution may be more close to the center frequency when there is no strong signal input.

As a result, the instantaneous frequency at the maximum amplitude is selected to represent the median frequency during the lightning period. The instantaneous frequencies at the maximum amplitudes of the lightning waveforms from similar distances are compared to determine the differences between individual events (Figure 5, right). As discussed above, a narrow frequency bandwidth of 4 kHz is chosen with a varying center frequency, in order to constrain the target frequency range around the same modal maximum in the spectrum. These varying center frequencies are selected from the maxima of the second modal peak, which always fall between 10-20 kHz in the spectrum, for example at 300 km, 350 km and 400 km distance. The instantaneous frequencies at the maximum amplitudes are calculated for all the waveforms recorded by one station, and the distribution of the instantaneous frequencies at the same distance bin is a clearly peaked distribution (Figure 5, right). This indicates that the instantaneous frequencies at one distance bin are range limited. The center frequencies associated with the main peaks of the distributions are clearly distance dependent as a result of the radio wave propagation. In other words, the instantaneous frequency inferred from the average lightning waveform can be used to represent the source receiver distance.

This idea can be tested by extending the analysis with the average lightning waveforms from 300-600 km at each distance bin separated by 10 km in the frequency range 10-20 kHz (Figure 6). The calculated instantaneous frequencies are obviously distance dependent and follow the second modal maximum in the spectra well. This excellent result strongly suggests that the instantaneous frequency has a promising potential application to determine the lightning distance from a single radio receiver.

6 Discussion and conclusion

The lightning waveform bank produced for distances up to 1000 km with a spatial resolution of 10 km is well suited for applications to study long range lightning location systems and electromagnetic wave propagation. For most lightning location systems, the baseline is smaller than 1000 km so that we can simulate and examine a new location algorithm or new site deployments. For wave propagation and ionospheric research, this waveform bank is valuable as a reference for modeling [*e.g. Pasko and Fullekrug, 2011*]. In particular, spectra have been calculated across a lightning waveform bank, that reveal a sequence of consecutive modal maxima depending on distance and frequency. This waveform bank is generated from lightning recordings of a thunderstorm in Europe, which may not be identical to waveform banks calculated for other geographical areas. The geometry of the experiment limits the waveform bank to propagation distances with less than 1000 km. However, the general method of producing the waveform bank and the spectral waveform bank is applicable to other locations and longer distance than 1000 km in the future. In addition, this method is also applicable to studies of other types of lightning, such as intra-cloud (IC) lightning discharges.

To the best of our knowledge, the complex waveform bank analysis of lightning is used for the first time, and it provides an opportunity to extract the instantaneous phase and instantaneous frequency. The distance discrimination with the instantaneous frequency is just one potential application of this complex waveform bank. The instantaneous frequency may also be discriminated by different arrival azimuths, elevation angles or different times of day, given more data. For example, it has been observed that a different incident elevation angle indicates a different rotation direction in the complex waveform of the lightning, i.e., a different instantaneous frequency [*Fullekrug et al., 2016, Figure 2, right*]. By using the instantaneous frequency for distance determination, the lightning signal can be first approximated within <50 km, because the instantaneous frequency can vary, e.g. between 400 km and 450 km distance (Figure 6). This uncertainty is very likely due to the lack of data at these distances, which could be improved by collecting more data with longer recordings. On the other hand, the instantaneous frequency is calculated from lightning waveforms that include interference from the local radio noise environment of each station. It is shown that the distribution of apparent frequencies from lightning at similar distances is a clearly peaked distribution if they are recorded at the same station (Figure 5, right). Between different stations, the distributions may differ slightly, most probably because of varying local radio environments and/or different propagation paths. As a result, the distance determination by using instantaneous frequency may be more accurate if the instantaneous frequencies are derived from each station separately. It is noted that the instantaneous frequency in maximum amplitude is equal to the amplitude weighted average frequency, such that waveform spectra inferred from STFT's with suitable parameters might result in similar distance dependencies.

In summary, this study has offered several results: (1) The average lightning sferic waveforms from different distances exhibit a sequence of consecutive maxima resulting from the ionospheric reflections, which can be used for radio propagation studies, lightning modeling, lightning detection simulation, etc. (2) In the spectral waveform bank, the sequence of consecutive modal maxima is separated by distinct minima at different frequencies and distances. (3) Long-range lightning location can achieve sub-sampling time accuracy by using the instantaneous phase of the complex lightning sferic waveform. (4) The instantaneous frequency calculated from average lightning waveforms has been shown to be distance dependent, and it therefore has the potential to be used for lightning distance determination.

Acknowledgments. The work of Z.L. is sponsored by the University of Bath, UK MetOffice (EA-EE1077) and the China Scholarship Council (CSC) (File No.201408060073). The work of K.K. is sponsored by the Engineering and Physical Sciences Research Council (EPSRC) under DTA contract EB-EE1151. The work of M.F. and A.M. is sponsored by the Natural Environment Research Council (NERC) under grants NE/L012669/1 and NE/H024921/1. This work was partly inspired by the SAINT project of the European Commission (H2020-MSCA-ITN-2016, 722337). The data used for this publication is available from https://doi.org/10.15125/BATH-00404. Z.L. wrote the paper and performed the data analysis, K.K. advised on the use of the Hilbert transform, A.M. assisted with the installation of the receiver network, S.E. and J.S. helped with the interpretation of the results, and M.F. supervised the work of Z.L. and advised on the concepts for the data analyses. The authors wish to thank Serge Soula, Jean-Louis Pincon, Stephane Gaffet and their teams for hosting the radio receivers in Lannemezan, Orleans and Rustrel. Z.L. wants to thank Dirk Klugmann and Ivan Astin for encouragement toward this project and acknowledges helpful discussions and support from Andrew Moss as well as the constructive suggestions of the anonymous reviewers.

References

Bitzer P. M., H. J. Christian, M. Stewart, J. Burchfield, S. Podgorny, D. Corredor, J. Hall, E. Kuznetsov, and V. Franklin (2013), Characterization and applications of VLF/LF source locations from lightning using the Huntsville Alabama Marx Meter Array, J. Geophys. Res. Atmos., 118,3120–3138, doi:10.1002/jgrd.50271.

Carvalho, F. L., M. A. Uman, D. M. Jordan, J. D. Hill, S. A. Cummer, D. A. Kotovsky, and R. C. Moore (2017), Triggered lightning sky waves, return stroke modeling, and ionosphere effective height, J. Geophys. Res. Atmos., 122, 3507–3527,

Cheng, Z., S. A. Cummer, H.-T. Su, and R.-R. Hsu (2007), Broadband very low frequency measurement of D region ionospheric perturbations caused by lightning electromagnetic pulses, J. Geophys. Res., 112, A06318, doi:10.1029/2006JA011840.

Cummins, K. L., M. J. Murphy, E. A. Bardo, W. L. Hiscox, R. B. Pyle, and A. E. Pifer (1998), A Combined TOA/MDF Technology Upgrade of the U.S. National Lightning Detection Network, J. Geophys. Res., 103(D8), 9035–9044, doi:10.1029/98JD00153.

Cummins, K., and M. Murphy (2009), An overview of lightning locating systems: History, techniques, and data uses, with an in-depth look at the US NLDN, IEEE Trans. Electromag. Compat., 51(3), 499–518, doi:10.1109/TEMC.2009.2023450.

Dowden, R. L., Brundell, J. B., Rodger, C. J. (2002), VLF lightning location by time of group arrival (TOGA) at multiple sites. Journal of Atmospheric and Solar-Terrestrial Physics 64(7): 817-830. doi:10.1016/S1364-6826(02)00085-8.

Füllekrug, M. and S. Constable (2000), "Global triangulation of intense lightning discharges." Geophysical Research Letters 27(3): 333-336, doi: 10.1029/1999GL003684.

Füllekrug, M., Mareev, E. and Rycroft, M. (2006), Sprites, elves and intense lightning discharges, Springer Science & Business Media, doi: 10.1007/1-4020-4629-4.

Füllekrug, M. (2010), Wideband digital low-frequency radio receiver, Meas. Sci. Technol., 21 (015901), 1–9, doi:10.1088/0957-0233/21/ 1/015901.

Fullekrug, M., et al. (2013), Electron acceleration above thunderclouds. Environmental Research Letters, 8 (3), 035027, doi: 10.1088/1748-9326/8/3/035027.

Füllekrug, M., A. Mezentsev, R. Watson, S. Gaffet, I. Astin, and A. Evans (2014), Array analysis of electromagnetic radiation from radio transmitters for submarine communication, Geophys. Res. Lett., 41, 9143–9149, doi:10.1002/2014GL062126.

Füllekrug, M., A. Mezentsev, R. Watson, S. Gaffet, I. Astin, N. Smith, and A. Evans (2015), Map of low-frequency electromagnetic noise in the sky. Geophys. Res. Lett., 42, 4648–4653. doi: 10.1002/2015GL064142.

Füllekrug, M., Z. Liu, K. Koh, A. Mezentsev, S. Pedeboy, S. Soula, S.-E. Enno, J. Sugier, and M. J. Rycroft (2016), Mapping lightning in the sky with a mini array, Geophys. Res. Lett., 43, 10,448–10,454, doi:10.1002/2016GL070737.

Höller, H., Betz, H.-D., Schmidt, K., Calheiros, R. V., May, P., Houngninou, E., and Scialom, G. (2009), Lightning characteristics observed by a VLF/LF lightning detection network (LINET) in Brazil, Australia, Africa and Germany, Atmos. Chem. Phys., 9, 7795-7824, doi: 10.5194/acp-9-7795-2009.

Horner, F. (1954), The accuracy of the location of sources of atmospherics by radio direction-finding, Proc IEEE 101: 383-390, doi: 10.1049/pi-3.1954.0091.

Horner, F. (1957), Very-low-frequency propagation and direction-finding, Proc IEEE 104: 73-80, doi: 10.1049/pi-b-1.1957.0118.

Kohlmann, H., W. Schulz, and S. Pedeboy (2017), Evaluation of EUCLID IC/CG classification performance based on ground-truth data. 2017 International Symposium on Lightning Protection (XIV SIPDA), Natal, Brazil, 2-6 Oct. 2017, doi: 10.1109/SIPDA.2017.8116896

Krider, E. P., R. Carl Noggle, and Martin A. Uman (1976), A Gated, Wideband Magnetic Direction Finder for Lightning Return Strokes. J. Appl. Meteor., 15, 301–306. doi: 10.1175/1520-0450(1976)015<0301:AGWMDF>2.0.CO;2.

Lee, A.C. (1986), An experimental study of the remote location of lightning flashes using a VLF arrival time difference technique, Q. J. Roy. Meteor. Soc., 112, 203–229, doi:10.1002/qj.49711247112.

Lee, A.C. (1990), Bias Elimination and Scatter in Lightning Location by the VLF Arrival Time Difference Technique. J. Atmos. Oceanic Technol., 7, 719–733, doi: 10.1175/1520-0426(1990)007<0719:BEASIL>2.0.CO;2

Liu, Z., K. L. Koh, A. Mezentsev, S.-E. Enno, J. Sugier, and M. Füllekrug (2016), Variable phase propagation velocity for long-range lightning location system, Radio Sci., 51, 1806–1815, doi:10.1002/2016RS006058.

Lyu, F., S. A. Cummer, R. Solanki, J. Weinert, L. McTague, A. Katko, J. Barrett, L. Zigoneanu, Y. Xie, and W. Wang (2014), A low-frequency near-field interferometric-TOA 3-D Lightning Mapping Array, Geophys. Res. Lett., 41, 7777–7784, doi:10.1002/2014GL061963.

Mezentsev, A., and M. Füllekrug (2013), Mapping the radio sky with an interferometric network of low-frequency radio receivers, J. Geophys. Res., 118, 8390–8398, doi:10.1002/jgrd.50671.

Nag, A, Murphy, MJ, Schulz, W, and Cummins, KL (2015), Lightning locating systems: Insights on characteristics and validation techniques. Earth and Space Science, 2, 65–93. doi: 10.1002/2014EA000051.

Pasko, V.P. and Fullekrug, M. (2011), Waveforms of Nighttime Atmospherics as a Measure of the Lower Ionospheric Electron Density Profiles over UK and France on August 31, 2008', paper presented to 30th URSI General Assembly (No. GHE2-7), Istanbul, Turkey, 13-20 August, viewed 24 July 2017, <http://www.ursi.org/proceedings/procGA11/ursi/GHE2-7.pdf>

Qin, Z., M. Chen, B. Zhu, and Y. Du (2017), An improved ray theory and transfer matrix method-based model for lightning electromagnetic pulses propagating in Earth-ionosphere waveguide and its applications, J. Geophys. Res. Atmos., 122, 712–727, doi:10.1002/2016JD025599.

Rakov, V. A. and M. A. Uman (2003), Lightning: physics and effects, Cambridge University Press. doi:10.1256/wea.168/03.

Rakov, V. (2013), "Electromagnetic methods of lightning detection." Surveys in Geophysics 34(6): 731-753. doi:10.1007/s10712-013-9251-1.

Rison, W., Krehbiel, P. R., Stock, M. G., Edens, H. E., Shao, X. M., Thomas, R. J., Stanley, M. A., Zhang, Y. (2016), Observations of narrow bipolar events reveal how lightning is initiated in thunderstorms." Nat Commun 7. doi:10.1038/ncomms10721.

Said, R. K., U. S. Inan, and K. L. Cummins (2010), Long-range lightning geolocation using a VLF radio atmospheric waveform bank, J. Geophys. Res., 115, D23108, doi:10.1029/2010JD013863.

Schonland, B. F. J., J. S. Elder, D. B. Hodges, W. E. Phillips, J. W. van Wyk (1940), The wave form of atmospherics at night. Proc. R. Soc. Lond. A 1940 176 180-202. doi: 10.1098/rspa.1940.0085.

Shao, X. M., Lay, E. H., & Jacobson, A. R. (2013). Reduction of electron density in the night-time lower ionosphere in response to a thunderstorm. Nature Geoscience, 6(1), 29-33. doi:10.1038/ngeo1668

Soula, S., Iacovella, F., van der Velde, O., Montanyà, J., Füllekrug, M., Farges, T., Bór, J., Georgis, J.-F., NaitAmor, S. and Martin, J.-M., (2014), Multi-instrumental analysis of large sprite events and their producing storm in southern France. Atmospheric Research 135: 415-431. doi:10.1016/j.atmosres.2012.10.004.

Stock, M. G., M. Akita, P. R. Krehbiel, W. Rison, H. E. Edens, Z. Kawasaki, and M. A. Stanley (2014), Continuous broadband digital interferometry of lightning using a generalized cross-correlation algorithm, J. Geophys. Res. Atmos., 119, 3134-3165, doi:10.1002/2013JD020217.

Sun, Z., X. Qie, M. Liu, R. Jiang, Z. Wang, and H. Zhang (2016), Characteristics of a negative lightning with multiple-ground terminations observed by a VHF lightning location system, J. Geophys. Res. Atmos., 121, 413–426, doi:10.1002/2015JD023702.

Taner, M. T., F. Koehler, R. E. Sheriff (1979), Complex seismic trace analysis. Geophysics 44(6): 1041-1063. doi: 10.1190/1.1440994.

Wang, Y., X. Qie, D. Wang, M. Liu, D. Su, Z. Wang, D. Liu, Z. Wu, Z. Sun, Y. Tian (2016), Beijing Lightning Network (BLNET) and the observation on preliminary breakdown processes, Atmos. Res. 171: 121-132. doi:10.1016/j.atmosres.2015.12.012

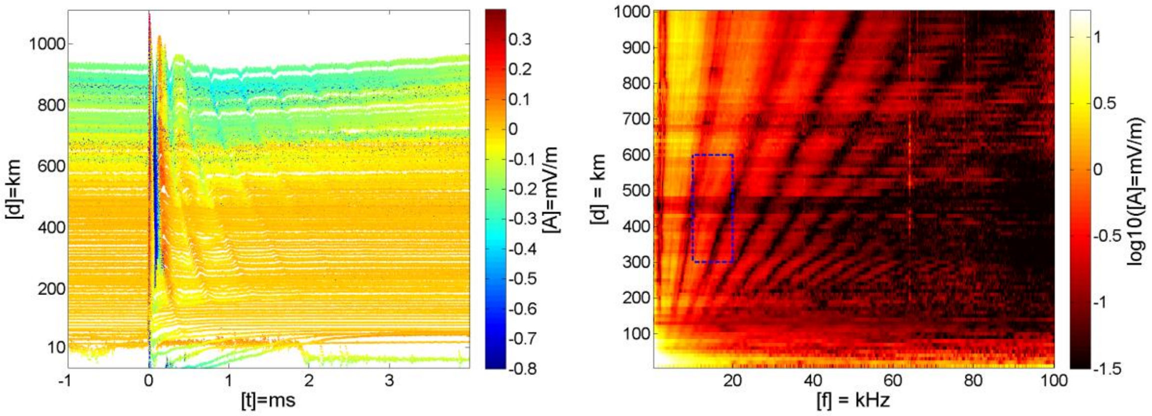

Figure 1. The average night-time waveforms and the spectra of the average waveforms of negative lightning discharges at distances from 10-1000 km. (left) Each average waveform at a given distance is calculated from more than one hundred events. The time axis is referenced to t=0 corresponding to a propagation at the speed of light from the source to the receiver. A sequence of consecutive maxima resulting from the ionospheric reflections (or multi-hop sky waves) appear from ~100 km distance onwards and the time differences between ground wave and sky waves are smaller for larger distances. (right) The sequence of consecutive modal maxima (yellow and red) is separated by distinct minima (black) which are characteristic for the distance between the radio receiver and the lightning discharge. The area of the blue square is used for the analysis of the instantaneous frequencies (compare to Figure 6).

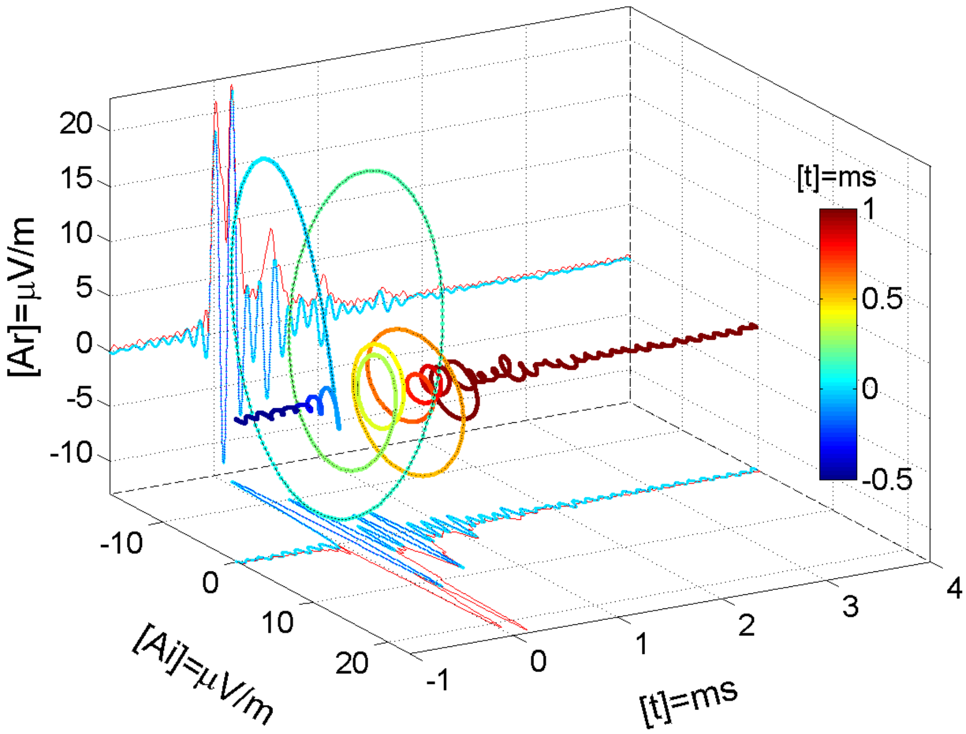

Figure 2. Isometric diagram of an average complex waveform of lightning at a distance of 300 km. The 3D trace of the complex lightning signal from 2 kHz to 18 kHz exhibits large amplitudes when the ground wave and sky waves are arriving. The rotation direction of the complex trace is anticlockwise, which means the instantaneous frequency is smaller than centre frequency. The blue lines show

the real part (A_r) and imaginary part (A_i) of the complex lightning waveform. The thin red line is the amplitude envelope of the complex waveform.

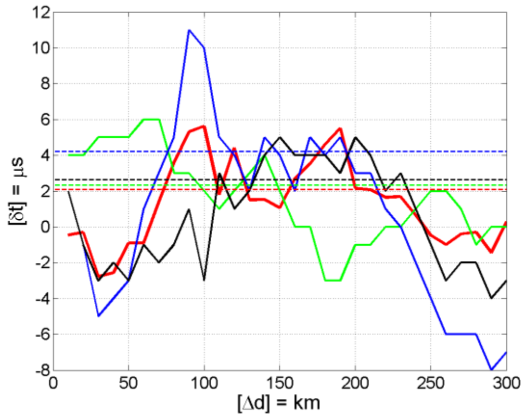

Figure 3. The time offsets between different propagation distance differences with respect to a speed of light propagation. The average lightning waveforms from 310 km to 600 km are compared with the average lightning waveform at 300 km distance. The time offset δt is the measured time difference Δt minus the nominal time difference inferred from a wave propagation velocity at speed of light Δd/c, and the distance differences Δd is measured relative to the lightning waveform at 300 km distance, i.e., Δd = d-300 km with d ranging from 310 km to 600 km. By comparing different signal processing methods, the average value of the absolute time offset by using the instantaneous phase of the complex lightning waveform (red) is less than just using the amplitude envelope (blue) or using the amplitude of the real signal (black) or cross correlating lightning waveforms (green). The corresponding average values of the absolute time offset are shown by the dashed lines.

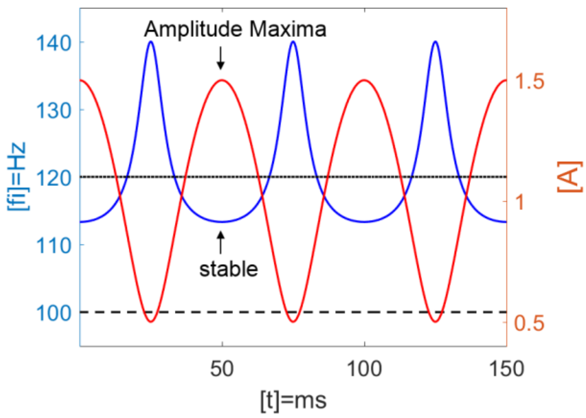

Figure 4. The instantaneous frequency of a simulated superposed signal that consists of two frequency components at 100 Hz and 120 Hz (black solid and dashed lines). The calculated instantaneous frequency of the averaged signal (blue line) is more stable and equal to the amplitude-weighted average value calculated by equation 7 when the amplitude is maximal (red line).

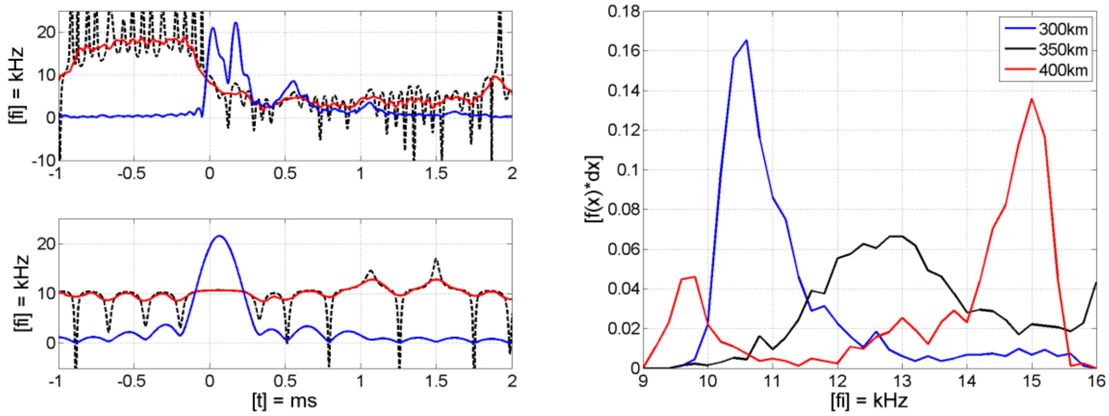

Figure 5. Analyses of instantaneous frequencies inferred from lightning waveforms. (left) The instantaneous frequency (black dashed line) calculated from a lightning waveform with two frequency bandwidths, 2-18 kHz (top) and 8.8-12.8 kHz (bottom), confirm the theoretical result that the instantaneous frequency is more stable when the amplitude of the signal is maximal (blue line). The amplitude weighted average instantaneous frequency (red line) smoothens the original instantaneous frequency. The instantaneous frequency calculated from a 4 kHz bandwidth around one modal maximum in the spectrum is less variable than using a bandwidth from 2-18 kHz that contains many modal maxima. (right) The distributions of the instantaneous frequencies at maximum amplitudes inferred from all the lightning waveforms recorded by one station at several distance bins are clearly peaked distributions.

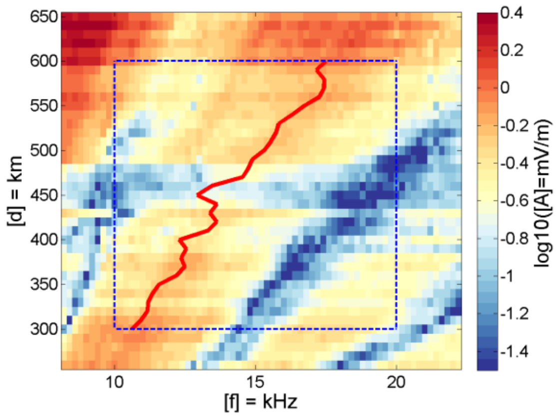

Figure 6. The instantaneous frequencies (red line) at maximum amplitudes of the average lightning waveforms at distances ranging from 300-600 km (blue square) follow the modal maximum in the spectra well.